An optimization study on adsorption of Reactive Blue 19 dye from aqueous solutions by extremely effective and reusable novel magnetic nanoadsorbent

Merve Pehlivan[a], Sinem Simsek[a], Sunullah Ozbek[b,*], Belma Ozbek[a,*]

[a]*Yildiz Technical University, Chemical Engineering Department, Davutpasa Campus, Esenler/Istanbul, 34220 Turkey,*
Tel. +90 212 383 4747; emails: bozbek@yildiz.edu.tr (B. Ozbek), mervep70@gmail.com (M. Pehlivan), sinemsimsekk@gmail.com (S. Simsek)
[b]*Mechanical Engineering Department, Doğuş University, Acibadem Campus, Kadıköy/Istanbul, 34722, Turkey,*
Tel. +90 444 79 97 Ext. 1201; email: sunullah.ozbek@gmail.com (S. Ozbek)

ABSTRACT

In the present study, the potential usage of iron-based magnetic aluminium oxide nanocomposite (IMANC) as a novel magnetic nanoadsorbent, which was synthesized by solution combustion method using a stoichiometric amount of glycine (100%) as fuel type, was investigated for the Reactive Blue 19 (RB19) dye removal from aqueous solutions by adsorption process. The synthesized IMANC sample found to have small particle size and high surface area with the porous structure according to the results obtained from the characterization studies performed. The dye adsorption process onto IMANC sample was optimized by applying the response surface methodology. For optimization studies, the experimental set was planned using an experimental design programme, Design Expert 11.0 trial software. The effects of pH, temperature and nanoadsorbent amount were investigated for RB19 dye removal from aqueous solutions. A model equation was developed using the Box–Behnken methodology. Additionally, the adsorption isotherm and kinetic models were examined according to the data obtained from the adsorption experiments performed at optimum process conditions. Moreover, the removal efficiencies of the regenerated IMANC synthesized were determined for each adsorption–desorption cycle. Even after the tenth adsorption–desorption cycle, the removal efficiency of the regenerated IMANC was maintained at approximately 96% of the initial efficiency which shows that the nanoadsorbent is extremely effective and reusable. Therefore, it was concluded that IMANC synthesized has great application potential in dye removal from aqueous solutions due to its desirable features such as high adsorption capacity, easy regeneration and adequate repeated uses.

Keywords: Magnetic nanoadsorbent; RB19; Experimental design; Adsorption; Desorption

1. Introduction

The dyestuffs and pigments are widely used in various industries; textile, food, paint, paper, plastic, cosmetics, food, leather, drug, rubber and etc. The release of various quantities of synthetic dyes and/or dye by-products into the water from several industrial areas during coloring and washing steps leads to environmental pollution problems. The synthetic dyes and pigments are non-biodegradable and toxic due to their aromatic rings in their structures [1–12]. Moreover, synthetic dyes usually consist of various contaminations including acids, bases, toxic compounds and color [13,14]. The release of synthetic dyes from various industries into water significantly threatens human health, animals, and

* Corresponding authors.

plants. Because, the synthetic dyes can cause some illness and disorders in reproductive systems, liver, brain, central nervous system and etc. [5,15,16].

Reactive Blue 19 (RB19) is an anionic dye and one of the most commonly used dyes in the industries of textile, carpet, plastic, cosmetic, food, leather, printing, paper, and etc. However, recent researches suggested that RB19 dye has mutagenic properties due to its electrophilic vinyl sulfone groups [17–19]. Moreover, the solubility of RB19 dye is high and its degree of fixation is low, which makes RB19 dye potential carcinogen and toxic. Therefore, it is important to provide a reliable and eco-friendly method for RB19 dye removal from wastewater [20,21].

There are several treatment techniques including chemical, physical and biological for removing the dyes from wastewater; adsorption [22], coagulation and/or flocculation [23], chemical oxidation [24], membrane separation [25], electrochemical degradation [26], microbial degradation [27], ozonation [28], ion-exchange [29] and etc. These methods apart from adsorption have several disadvantages like the utilization of synthetic chemicals, the formation of undesired products, being expensive and etc. On the other hand, the adsorption technique is a commonly preferred and more versatile technique among the other techniques used in wastewater treatment due to its simple operation, inexpensiveness, eco-friendliness, pH tolerance, easier recovery of adsorbent and high-quality of the treated effluents. Additionally, the adsorption process does not require huge investment and/or energy source which are undesirable facts for the treatment of wastewater [30–34].

The adsorption process of dyes is related to the properties of dyes and the surface chemistry of adsorbent used. Moreover, the process conditions of aqueous solution; temperature, pH, adsorbent amount, initial dye concentration and etc., play the main role in the dye adsorption process effectiveness.

As reported in the study performed by Salleh et al. [31], the pH value of the solution affects the adsorption of anionic and cationic dyes differently. For cationic dye adsorption at high pH values, the positive charge at the solution interface decreases and the adsorbent surface charged negatively. Therefore, the cationic dye adsorption increases unlike anionic dye adsorption. Oppositely, for anionic dye adsorption at lower pH values, the positive charge on the solution interface increases and the adsorbent surface charged positively. Thus, the anionic dye adsorption increases unlike cationic dye adsorption. Consequently, for cationic dye adsorption, high pH values are required, but for anionic dye adsorption, lower pH values are required [31].

In the literature, the various studies on RB19 dye (anionic dye) removal from aqueous solutions for wastewater treatment were performed by using agricultural and industrial wastes, organic or inorganic based materials as adsorbents. For example; several adsorbents used for RB19 dye removal are as follows; modified and non-modified orange peel [18], lignocellulosic waste [35], nanostructured magnesium oxide particles [36], activated carbon [1], multi-walled and single-walled carbon nanotubes [37], chitosan-coated magnetic hydroxyapatite nanoparticles [2], jujube stems powder [38], NiO nanoparticles [39], pomegranate seeds powder [5], *Lemna minor* [21], alumina/carbon nanotube [40],

rice straw fly ash [41], multi-walled carbon nanotubes [42], L-arginine-functionalized Fe_3O_4 nanoparticles [43], hydroxyapatite (HAp) nanopowders [44], wheat straw [13], peanut shell [45], *Panus tigrinus* [17], chitosan/SiO_2/carbon nanotubes [46], modified silica gel [47], chitosan-based magnetic adsorbent [22], graphene oxide modified with polystyrene [48] and etc.

The magnetic nanocomposites indicate high saturation magnetization and high coercivity [49]. Therefore, several researchers have studied the synthesis of magnetic nanocomposites and analyzed their properties [50–53]. The separation process of iron based magnetic aluminium oxide nanocomposite (IMANC) from the liquid phase becomes easy by applying a magnetic field due to their magnetic properties [54,55]. In this sense, IMANC samples have gained increasing attention for their usage as effective nanoadsorbents and magnetic supports in the environmental and biotechnological areas [56–58]. In addition to high adsorption capacity, regeneration and efficient separation of magnetic nanocomposites are also important properties. Magnetic separation method has features such as high efficiency, low cost and eco-friendly compared to traditional centrifugation and filtration methods. Therefore, the numerous studies were found on the usage of magnetic nanocomposites as nanoadsorbents for the dye removal process, in the literature [2,22,59–61].

The experimental design is a structured and systematic approach for the determination of the effects of experimental variables on the system [62,63]. Because, the conventional and classical methods are time consuming, and require lots of experiments for the determination of optimum conditions. The limitations of these methods can be eliminated by optimization of the process parameters using an experimental design like response surface methodology (RSM) [64,65]. RSM is the combination of mathematical and statistical methods for modelling of engineering problems, and that can be used for evaluation of the significance of several factors in complex interactions [66,67]. So, optimization of adsorption process conditions by RSM will greatly help to progress of the industrial-scale dye removal treatment [31,68]. The most common and efficient technique used for RSM is called Box–Behnken design [69].

The novel magnetic nanoadsorbent samples, IMANC coded as SC-FA-G2 (solution combustion –$Fe(NO_3)_3$/$Al(NO_3)_3$ - glycine 100%), were synthesized by solution combustion method, which is an easy, quick and low-cost method for fabrication of nanosized materials, as reported in our previous study [70]. After the evaluation of data obtained from the characterization studies, SC-FA-G2 found to have the high surface area with a porous structure and small particle size which are the desirable features for the adsorption process. In the present study, it was planned to examine the potential usage of SC-FA-G2 sample as a novel magnetic nanoadsorbent for RB19 dye removal from aqueous solutions for wastewater treatment.

For the adsorption process, the experimental set was planned using a Design Expert 11.0 trial software experimental design programme according to the RSM. The experimental conditions were defined according to the reports demonstrated in the literature on the adsorption of RB19 dye. The pH range was chosen between 2 and 6, because of the

higher uptake rate of RB19 dye in lower pH values [18,71,72]. Similarly, the temperature range was selected between 25°C and 45°C [72,73]. For the investigation of RB19 dye removal capacity of the nanoadsorbent used (SC-FA-G2) from aqueous solutions, the set of experiments were conducted under the following process conditions such as pH values of 2, 4 and 6, temperature values of 25°C, 35°C and 45°C and nanoadsorbent amounts of 200, 400 and 600 mg/50 mL. According to data collected from adsorption experiments, the adsorption isotherm models (Langmuir, Freundlich, and Temkin) and the kinetic models (pseudo-first-order, pseudo-second-order, Elovich and intraparticle diffusion) were examined at the optimum process conditions obtained. In addition, the effectiveness and reusability features of the regenerated novel magnetic nanoadsorbent (SC-FA-G2) were evaluated for each adsorption–desorption cycle.

2. Experimental

2.1. Materials

Aluminium nitrate nonahydrate ($Al(NO_3)_3 \cdot 9H_2O$) and iron (III) nitrate nonahydrate ($Fe(NO_3)_3 \cdot 9H_2O$) were purchased from Merck, Germany. Glycine ($NH_2CH_2CO_2H$) was purchased from Alfa Aesar, United Kingdom. RB19 dye was supplied by Sigma-Aldrich, Germany. The chemical structure of RB19 dye used is represented in Fig. 1. The chemicals were utilized without any further purification (Table 1). The specified amount of dye was added into distilled water for the preparation of the aqueous solution.

2.2. Studies on synthesis and characterization of magnetic nanoadsorbent

The novel magnetic nanoadsorbent sample, IMANC, coded as SC-FA-G2, was synthesized by solution combustion method as reported in our previous study [70]. The details of the characterization studies on the synthesized SC-FA-G2
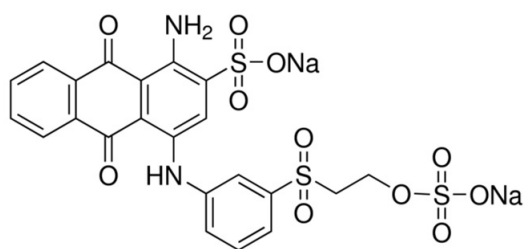

Fig. 1. Chemical structure of Reactive Blue 19 dye used.

by scanning electron microscopy, Fourier transform infrared analysis, X-ray diffraction, thermogravimetric and differential thermal analysis, and surface area-porosity analyzer can be found in the previously reported study [70]. In this study [70], SC-FA-G2 (solution combustion – $Fe(NO_3)_3$/$Al(NO_3)_3$ – glycine 100%) found to have small particle size at approximately 60 nm and porous structure mostly in spherical particle shape. From Brunauer–Emmett–Teller analysis, the surface area was found as 19.69 m^2/g. The pore sizes of SC-FA-G2 were approached to 18.7 and 14.8 nm after adsorption and desorption analysis by the Barrett, Joyner, and Halenda (BJH) method, respectively [70].

2.3. Studies on dye adsorption

The schematic view of the experimental procedure is represented in Fig. 2. The experimental set of RB19 dye adsorption was planned via Design Expert 11.0 trial software, an experimental design programme based on the RSM. The effects of parameters on adsorption of RB19 dye onto IMANC coded as SC-FA-G2 was investigated using a three-level Box–Behnken design method. The factor levels were coded as –1 (low), 0 (central point) and 1 (high). According to the data from Box–Behnken Design, 17 experiments were resumed to optimize the process parameters such as pH, temperature and nanoadsorbent amount for RB19 dye removal efficiency of SC-FA-G2 used.

Adsorption experiments were performed by the addition of magnetic nanoadsorbent into Erlenmeyer flask containing 50 mL of RB19 dye solution (100 ppm) at defined pH and temperature values. The effects of pH (2, 4, and 6), temperature (25°C, 35°C, and 45°C) and nanoadsorbent amount (4, 8, and 12 g/L) on the dye adsorption process were investigated. The initial pH of the dye solution was adjusted with the solutions of 1 M HCl or 0.1 M NaOH. The flasks were shaken in an orbital shaker at 100 rpm for 60 min. During the experiments, the samples were withdrawn from the flasks at defined time intervals. Then, the dye molecules adsorbed onto magnetic nanoadsorbent were removed from the solution easily by using a commercially available neodymium (NdFeB) magnet.

The optical densities of the samples were measured via a UV-Vis spectrophotometer at 592 nm wavelength for determination of remaining RB19 dye concentration. All experiments were run at least in duplicate, and the average of the measurements was taken. The reproducibility between the trials was within ±5%.

The dye adsorption capacities (q_e, mg/g) and dye removal rate percentage, $R_{Dye\ Removal}$ (%), were calculated using Eqs. (1) and (2), respectively.

Table 1
Specifications of the chemicals used

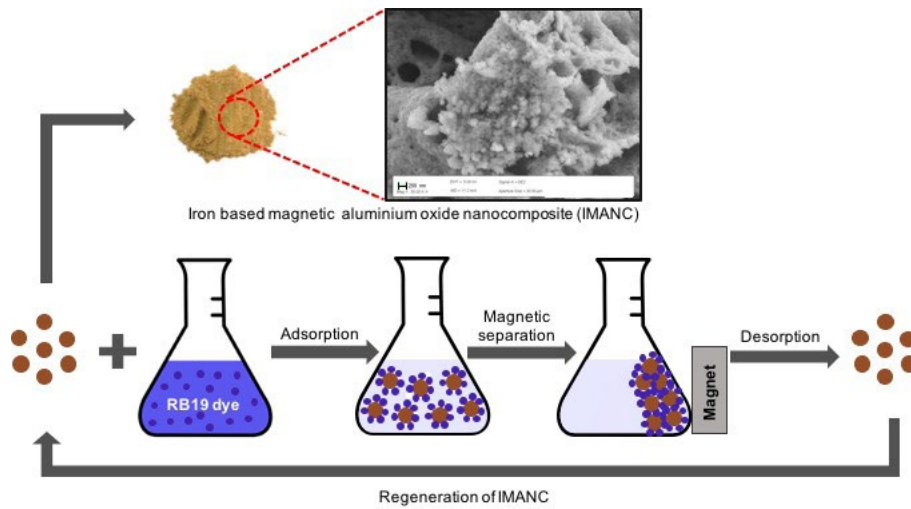| Component	Chemical formula	CAS registry number	Mass fraction purity	Suppliers
Aluminum nitrate nonahydrate	$Al(NO_3)_3 \cdot 9H_2O$	7784–27–2	≥98.5%	Merck, Germany
Iron(III) nitrate nonahydrate	$Fe(NO_3)_3 \cdot 9H_2O$	7782–61–8	99%–101%	Merck, Germany
Glycine	$NH_2CH_2CO_2H$	56–40–6	99%	Alfa Aesar, United Kingdom
Reactive Blue 19	$C_{22}H_{16}N_2Na_2O_{11}S_3$	2580–78–1	99%	Sigma-Aldrich, Germany

Fig. 2. Schematic view of the experimental procedure.

$$q_e = \frac{(C_0 - C_e) \times V}{m} \qquad (1)$$

$$R_{\text{Dye Removal}}(\%) = \frac{(C_0 - C_e)}{C_0} \times 100 \qquad (2)$$

where the initial and final (equilibrium) dye concentrations are C_0 and C_e (mg/L), respectively. The volume of the dye solution is V (L), and m (g) is the amount of adsorbent used.

2.4. Studies on dye desorption capability and reusability of magnetic nanoadsorbent

Dye desorption capability and repeated uses of SC-FA-G2 as a nanoadsorbent were investigated at optimum conditions as performed successive adsorption–desorption cycles. The adsorption studies were performed by the addition of 400 mg nanoadsorbent into a 50 mL RB19 dye solution. Then, the solution was mixed at 100 rpm for 60 min of processing time at a pH of 2 and a temperature of 25°C. After the adsorption process, SC-FA-G2 was separated from aqueous solution by a commercially available neodymium (NdFeB) magnet. Then, recovered SC-FA-G2 was transferred into 50 mL of NaOH solution (0.1 M) for desorption studies. After 5 min of desorption time, the absorbance value of RB19 dye remained in the solution was measured via a UV-Vis spectrophotometer. The same procedure was followed for each adsorption–desorption cycle experiment conducted. The adsorption and recovery steps were repeated after 10 cycles. 4% loss of adsorption capacity (remaining 96%) was found even after 10 repeated adsorption–desorption cycles. The images of SC-FA-G2 before and after the RB19 dye adsorption process were represented in Figs. 3a and b, respectively.

3. Results and discussions

3.1. Box–Behnken design method analysis for dye adsorption data

Using the Box–Behnken design method, 17 experiments were performed for investigation of the effects of process parameters; pH ($X1$), temperature (T: $X2$) and nanoadsorbent amount (AD: $X3$), for 60 min of processing time. The coefficients of the response function for process parameters were determined via Design Expert 11.0 trial software. The Box–Behnken design matrix and experimental responses for RB19 dye adsorption onto SC-FA-G2 were represented in Table 2.

The removal percentages of five experiments at the central point (at pH of 4, temperature of 35°C and nanoadsorbent amount of 400 mg SC-FA-G2/50 mL) were found very close to each other and associated with minimization of experimental errors. The minimum dye removal percentage was determined as 25 at the following conditions; pH of 6, 35°C, and 200 mg SC-FA-G2/50 mL. The maximum dye removal (100%) was determined at the following process conditions; (i) pH of 2, temperature of 25°C and 400 mg SC-FA-G2/50 mL; (ii) pH of 2, temperature of 35°C and 600 mg SC-FA-G2/50 mL; and (iii) pH of 2, temperature of 45°C and 400 mg SC-FA-G2/50 mL.

Considering the lower energy and nanoadsorbent amount requirements; the optimum process conditions for the achievement of 100% dye removal; pH, temperature and nanoadsorbent amount were chosen as 2, 25°C, and 400 mg/50 mL, respectively. After the evaluation of the experimental data, the quadratic model, Eq. (3), was developed using the Box–Behnken design method. ANOVA analysis data for the quadratic model developed is represented in Table 3.

$$\begin{aligned}
R_{\text{Dye Removal}}(\%) = {} & 63 - 21(\text{pH:}X1) + 5.38(\text{T:}X2) + 22.38(\text{AD:}X3) + \\
& 6.25(\text{pH:}X1)(\text{T:}X2) + 15.75(\text{pH:}X1)(\text{AD:}X3) - \\
& 1.5(\text{T:}X2)(\text{AD:}X3) + 12(\text{pH:}X1)^2 + 1.25(\text{T:}X2)^2 \\
& + 3.75(\text{AD:}X3)^2 \qquad (3)
\end{aligned}$$

According to the coefficients of process parameters of the response function developed [Eq. (3)], it was concluded that the temperature and nanoadsorbent amount have a positive influence on RB19 dye removal. The coefficients of determination R^2 and adjusted R^2 of the model were obtained as 0.9783 and 0.9505, respectively. The difference between

Fig. 3. Images of SC-FA-G2 (a) before and (b) after the RB19 dye adsorption process.

Table 2
Box–Behnken experimental design matrix and experimental responses of RB19 dye adsorption onto SC-FA-G2

RUN	$X1$ pH	$X2$ Temperature (°C)	$X3$ Nanoadsorbent amount (mg/50 mL)	R Dye removal (%)
1	6	45	400	65
2	6	35	600	95
3	4	35	400	58
4	4	35	400	60
5	4	35	400	63
6	2	35	200	93
7	4	45	200	48
8	2	25	400	100
9	2	45	400	100
10	6	25	400	40
11	4	35	400	66
12	2	35	600	100
13	6	35	200	25
14	4	25	600	90
15	4	35	400	68
16	4	45	600	96
17	4	25	200	36

predicted and experimental data was found as reasonably small, indicating the model adequacy to the response. A comparison of the predicted values vs. actual ones of RB19 dye removal percentages is illustrated in Fig. 4.

The analysis of variance (ANOVA) for Eq. (3) developed was represented in Table 3. The significance of process variables was checked by F-value and P-value. As given in Table 3, the F-value of the Model (35.13) states that the model is significant. P-values less than 0.001 mean that the model terms are significant. The terms of $X1$, $X2$, $X3$, $X1X3$ and $X1X1$ were significant, with very small P-values (P-values < 0.05). The lack of fit F-value of 2.84 indicates the

significance of the model correlation between the variables and the adsorption of RB19 dye. The lack of fit F-value is not significant as P-value is higher than 0.05. Therefore, all these results indicated that the model developed was applicable for the present study [1,69,74].

3.2. Effect of process variables

Three-dimensional response surface plots were constituted with the Design Expert 11.0 trial software experimental design programme presenting the effects and their interactions on the parameters of the RB19 dye adsorption process

Table 3
ANOVA analysis data for the quadratic model developed

| Source	Sum of squares	df	Mean square	F-value	P-value
Model	9,610.31	9	1,067.81	35.13	<0.0001
A-pH ($X1$)	3,528.00	1	3,528.00	116.08	<0.0001
B-Temperature ($X2$)	231.13	1	231.13	7.60	0.0282
C-Nanoadsorbent amount ($X3$)	4,005.13	1	4,005.13	131.78	<0.0001
AB	156.25	1	156.25	5.14	0.0577
AC	992.25	1	992.25	32.65	0.0007
BC	9.00	1	9.00	0.2961	0.6032
A^2	606.32	1	606.32	19.95	0.0029
B^2	6.58	1	6.58	0.2165	0.6559
C^2	44.47	1	44.47	1.46	0.2657
Residual	212.75	7	30.39		
Lack of fit	144.75	3	48.25	2.84	0.1697
Pure error	68.00	4	17.00		
Total	9,823.06	16			
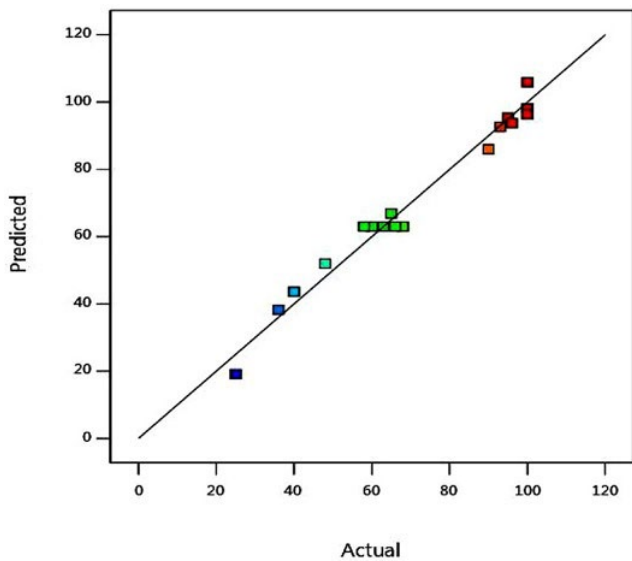
Fig. 4. Predicted data vs. actual data of RB19 dye removal percentage.

(Figs. 5a–c). As can be seen from Figs. 5a and b, the decrease in pH resulted in the increase for RB19 dye removal percentage. From Figs. 5b and c, the removal percentage of RB19 dye increased with ascending nanoadsorbent amount arising from the presence of more surface area of the nanoadsorbent.

Additionally, F-values can be used for the determination of the significance of the terms or components in the model developed [74,75]. Table 3 shows that the parameters of pH and nanoadsorbent amount are the most significant ones on the dye removal process as they have high F-values while the temperature is a less significant parameter as it has lower F-value compared to others.

As reported in the literature [31], the pH of the solution controls the magnitude of electrostatic charges which are imparted by dye molecules. Then, this will cause electrical interactions between dye molecules and adsorbent [31,76]. Similarly, in the present study, pH has a dramatic effect on the adsorption process. Therefore, electrical interactions seem to play an important role on the adsorption process. Additionally, the adsorption process may also be affected by mechanical trapping of dye molecules onto the surface of the porous structure of nanoadsorbent used.

3.3. Effect of processing time on dye removal process

The effect of processing time on RB19 dye removal is represented in Fig. 6. According to the data represented in Fig. 6, RB19 dye removal percentages were achieved as 96.2, 96.7, 98.8, and 100 at the processing times of 5, 10, 30, and 60 min, respectively. Although 96.2% of dye was removed in the first 5 min of the processing time, no fluctuations were observed during 60 min of the processing time.

3.4. Adsorption isotherm models

The distribution of the dye molecules at equilibrium between liquid and solid phases can be determined using adsorption isotherm models. Moreover, adsorption isotherm is important for the evaluation of the adsorption capacity [31]. The experimental data of RB19 dye adsorption onto SC-FA-G2 were examined by three most common adsorption isotherm models; namely Langmuir, Freundlich, and Temkin; which were illustrated at Eqs. (4)–(6), respectively.

$$\frac{C_e}{q_e} = \frac{C_e}{q_m} + \frac{1}{bq_m} \tag{4}$$

$$\ln q_e = \ln k_f + \frac{\ln C_e}{n} \tag{5}$$

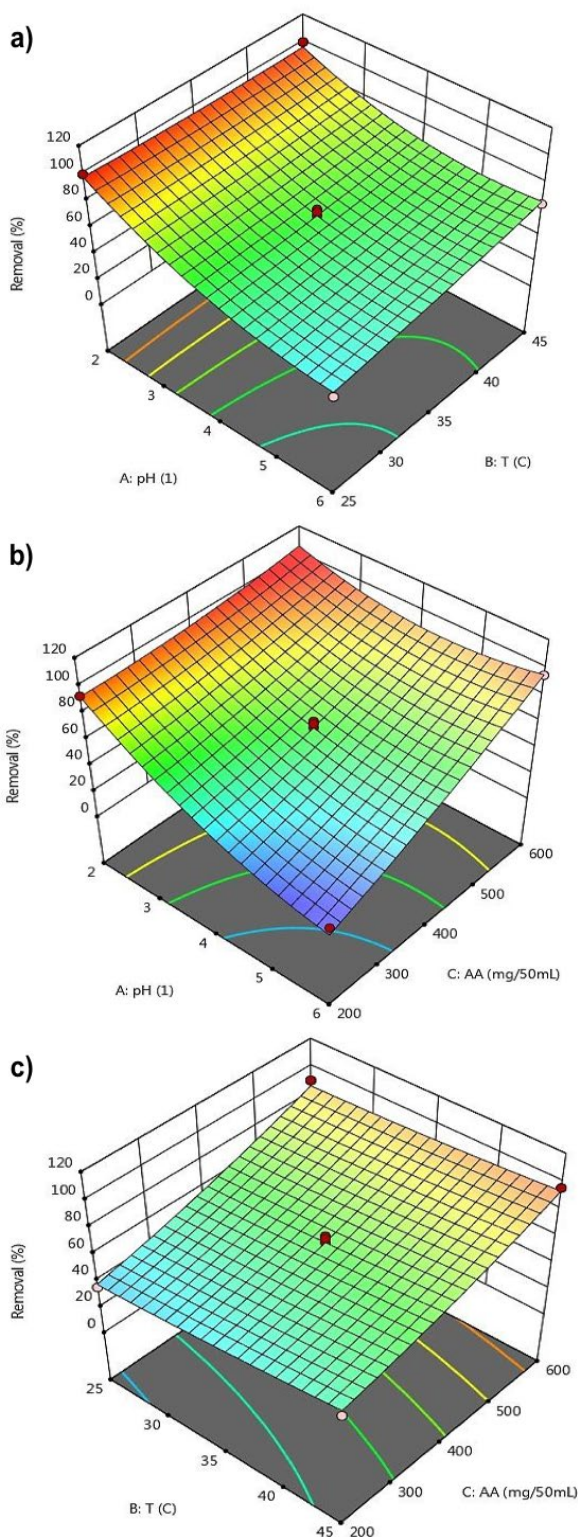$$q_e = \frac{RT}{b_T}\ln A_T + \frac{RT}{b_T}\ln C_e \tag{6}$$

Fig. 5. Three-dimensional response surface plots for the combined effects of (a) pH and temperature, (b) pH and nanoadsorbent amount, and (c) temperature and nanoadsorbent amount on RB19 dye removal percentage.
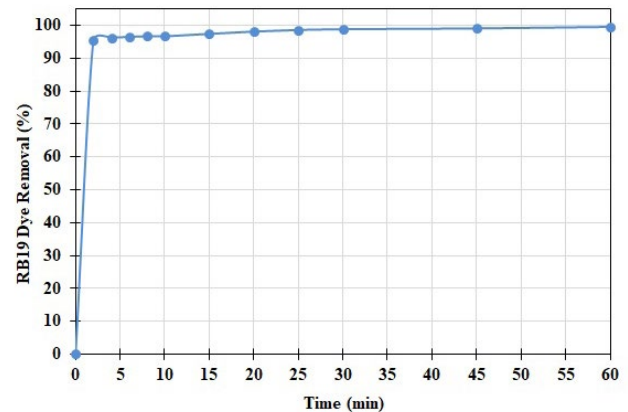

Fig. 6. Effect of processing time on RB19 dye removal for process conditions of pH 2, temperature of 25°C and nano adsorbent amount of 400 mg/50 mL.

where q_e (mg/g) is adsorption capacity at equilibrium, C_e (mg/L) is concentration of adsorbate at equilibrium, q_m (mg/g) is maximum adsorption capacity of adsorbent, b (L/mg) is Langmuir adsorption constant related to adsorption energy, k_f (mg$^{1-1/n}$L$^{1/n}$g^{-1}) is Freundlich affinity coefficient, n is Freundlich exponential coefficient, R (8.314 J/mole K) is ideal gas constant, T (K) temperature, b_T (J/mole) is Temkin constant related to adsorption temperature, and A_T (L/g) Temkin isotherm equilibrium binding constant.

The adsorption isotherm parameters, correlation coefficient (R^2) and standard deviation (σ) values calculated from experimental data were represented in Table 4. According to the data obtained, the Langmuir isotherm model was found as the most suitable model with the higher value of correlation coefficient (R^2) and lower value of the standard deviation (σ) (Fig. 7) comparison to Freundlich and Temkin isotherm models examined, as stated in the studies for RB19 dye adsorption non-modified orange peel [18], lignocellulosic waste [35], nanostructured magnesium oxide particles [36], jujube stems powder [38], *Lemna minor* [21], hydroxyapatite nanopowders [44], activated carbon [13], peanut shell [45], *Panus tigrinus* [17], chitosan/SiO$_2$/carbon nanotubes [46], modified silica gel [47], chitosan-based magnetic adsorbent [22] and etc. Langmuir isotherm model suggests that the RB19 dye adsorption onto SC-FA-G2 as novel magnetic nanoadsorbent is monolayer in nature as also stated by Xu et al. [22]. Even though, Temkin isotherm model has a high correlation coefficient value that did not describe very well the data of RB19 dye adsorption onto SC-FA-G2 due to its high standard deviation value ($\sigma = 0.8497$). Similarly, the Freundlich isotherm model was not found as an appropriate model for defining the adsorption data of RB19 dye as its standard deviation value ($\sigma = 0.1076$) found higher than the value ($\sigma = 0.0275$) obtained for Langmuir isotherm model (Table 4).

Additionally, the essential characteristics of Langmuir isotherm can be distinguished in terms of dimensionless separation factor, R_L defined as [5,44,48,77]:

$$R_L = \frac{1}{\left(1 + b \cdot C_0\right)} \tag{7}$$

Table 4
Estimated parameters and statistical values of adsorption isotherm models used for RB19 dye adsorption onto SC-FA-G2 at the process conditions of pH of 2, the temperature of 25°C and at various nanoadsorbent amounts from 50 to 400 mg in 50 mL

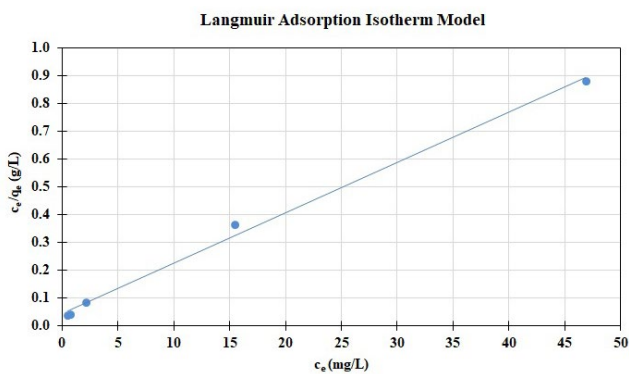| Adsorption isotherm models	Estimated parameters			
Langmuir	q_m (mg/g)	b (L/mg)	R^2	σ
	55.2486	0.4067	0.9956	0.0275
Freundlich	k_f (mg$^{1-1/n}$L$^{1/n}$g^{-1})	n	R^2	σ
	17.6617	3.2884	0.9768	0.1076
Temkin	A_T (L/g)	b_T (J/mole)	R^2	σ
	8.7938	284.0308	0.9982	0.8497

Fig. 7. Langmuir adsorption isotherm model data of RB19 dye removal onto SC-FA-G2.

where C_0 is the initial dye concentration (mg/L). The value of separation factor, R_L, refers whether the isotherm is favorable ($0 < R_L < 1$), unfavorable ($R_L > 1$), linear ($R_L = 1$) or irreversible ($R_L = 0$) [5,44,48,77]. In the present study, for Langmuir isotherm, R_L value was calculated as 0.024 which is between 0 and 1, suggesting that the RB19 dye adsorption process onto SC-FA-G2 magnetic nanoadsorbent was favorable.

Isotherm models can be used as a guide for investigation of the adsorption mechanism. In the study performed by Iqbal and Ashiq [78], Azizi et al. [48] and Vijayalakshmi et al. [79], it was reported that the adsorption data that fit the Langmuir isotherm model can be associated with the chemical adsorption. In the present study, the Langmuir isotherm model was determined as the most appropriate model with a higher value of correlation coefficient ($R^2 = 0.9956$) and a lower value of standard deviation ($\sigma = 0.0275$) for the adsorption data of RB19 dye onto SC-FA-G2. This result supports that the possible mechanism of the adsorption process may be the chemisorption.

On the other hand, it was also reported that the Freundlich parameter ($1/n$) in Eq. (5) might give information about the adsorption mechanism. As reported in the study performed by Dehvari et al. [5], the Freundlich parameter ($1/n$) may be associated with the mechanism of the adsorption process. Additionally, if $1/n$ value is smaller than 1, the adsorption process is controlled by chemisorption. In the present study, the Freundlich parameter ($1/n$) was calculated as 0.3041 less than 1, with the correlation

coefficient of R^2 of 0.9768 and the standard deviation of σ of 0.1076. Although the Freundlich model is not the best fitted model among others examined, this result found here indicates that the possible mechanism of the adsorption process of RB19 dye onto SC-FA-G2 may be associated with the chemisorption.

Temkin isotherm model may also be helpful for the prediction of the adsorption mechanism. In the study performed by Ahmed et al. [18], it was reported that Temkin constant, b, is related with the heat of sorption (J/mole), and if b value is higher than 45 J/mole, the adsorption process can be chemical in nature. In the present study, the values of the regression coefficient and the standard deviation of the Temkin isotherm model were found as $R^2 = 0.9982$ and $\sigma = 0.8497$. The heat of adsorption was calculated as 284.03 J/mole which is higher than 45 J/mole. Although the Temkin model is not the best fitted model among others examined, this result found here suggesting that the mechanism of adsorption may be associated with the chemisorption.

3.5. Adsorption kinetic models

As the determination of the adsorption kinetic is highly important for planning and controlling of adsorption process [31], adsorption kinetic studies were performed for calculation of the adsorption rate using adsorbate concentration at a specific time. For RB19 dye removal onto SC-FA-G2 by adsorption, the experimental data were evaluated by adsorption kinetic models; pseudo-first-order, pseudo-second-order, Elovich, and intraparticle diffusion models, which were illustrated at Eqs. (8)–(11), respectively.

$$\log\left(q_e - q_t\right) = \log q_e - \frac{k_1}{2.303}t \tag{8}$$

$$\frac{t}{q_t} = \frac{1}{k_{p2} \cdot q_e^2} + \frac{1}{q_e}t \tag{9}$$

$$q_t = \frac{1}{\beta}\ln\left(\alpha\beta\right) + \frac{1}{\beta}\ln t \tag{10}$$
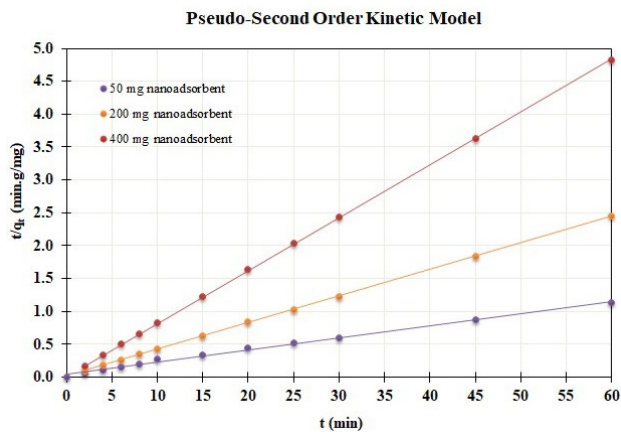
$$q_t = k_i t^{0.5} + c_i \tag{11}$$

Fig. 8. Linearized pseudo-second-order kinetic model used for the nanoadsorbent amounts of 50, 200, and 400 mg in 50 mL.

where q_e (mg/g) is adsorption capacity at equilibrium, q_t (mg/g) is adsorption capacity at time t, k_1 (1/min) is pseudo-first-order adsorption rate constant, k_{p2} (g/mg min) is pseudo-second-order adsorption rate constant, α (mg min/g) is initial adsorption rate, β (g/mg) is constant related to extent of surface coverage and activation energy, k_i intraparticle diffusion rate constant (mg/g min^2) and c_i is a constant related to layer thickness (mg/g).

The adsorption kinetic parameters, the values of correlation coefficient (R^2) and standard deviation (σ) are represented in Table 5. According to the data obtained, the pseudo-second-order kinetic model was determined as the most agreeable kinetic model with the high value of correlation coefficient (R^2) and low value of the standard deviation (σ) among other models examined (Fig. 8) (Table 5) as stated in the studies for RB19 dye adsorption onto modified and non-modified orange peel [18], lignocellulosic waste

[35], jujube stems powder [38], NiO nanoparticles [39], pomegranate seeds powder [5], *Lemna minor* [21], alumina/carbon nanotube [40], rice straw fly ash [41], L-arginine-functionalized Fe_3O_4 nanoparticles [43], hydroxyapatite nanopowders [44], wheat straw [13], peanut shell [45], *Panus tigrinus* [17], chitosan/SiO$_2$/carbon nanotubes [46], chitosan-based magnetic adsorbent [22], and etc.

As reported in the literature [5,22,31,80,81], pseudo-second-order kinetic may be associated with the chemically rate-controlling adsorption which called chemisorption. In the present study, pseudo-second-order kinetic model was found as the most appropriate model with a higher value of correlation coefficient ($R^2 = 0.9999$) and a lower value of standard deviation ($\sigma = 0.0045$) for the evaluation of the adsorption data of RB19 dye onto SC-FA-G2. Therefore, the adsorption may be associated with the chemisorption because of the kinetic data following the pseudo-second-order kinetic.

3.6. Activation energy calculation by Arrhenius relationship

Arrhenius equation can be used for the prediction of adsorption mechanism as stated in the studies performed by Ciobanu et al. [44], Mahmoud [82], Unuabonah et al. [83]. The linear form of the Arrhenius equation is expressed as:

$$\ln k_{p2} = \ln A - \left(\frac{E_a}{RT} \right) \tag{12}$$

where E_a represents the activation energy of the adsorption process, k represents the kinetic rate constant of the adsorption process, A represents the temperature-independent factor in (g/mg min), the universal gas constant R is 8.314 J/mole K and T is temperature in Kelvin. The value of activation energy (E_a) can be calculated from the plot of $\ln k$ vs. $1/T$ graph which was obtained for the best fitting kinetic

Table 5
Estimated parameters and statistical values of adsorption kinetic models for RB19 dye adsorption onto SC-FA-G2 at the process conditions of pH of 2, the temperature of 25°C and at various nanoadsorbent amounts from 50 to 400 mg in 50 mL

| Kinetic model equations	Estimated parameters	Nanoadsorbent amount		
		50 mg/50 mL	200 mg/50 mL	400 mg/50 mL
Pseudo-first-order	k_1, min^{-1}	0.0599	0.1559	0.0778
	R^2	0.9277	0.8732	0.5929
	σ	0.1222	0.2781	0.4085
Pseudo-second-order	k_{p2}, g mg^{-1} min^{-1}	0.0184	0.0911	0.3333
	R^2	0.9972	0.9999	0.9999
	σ	0.0185	0.0045	0.0077
Elovich	α, mg g^{-1} min	407.5982	3.1×10^9	7.3×10^{31}
	β, g mg^{-1}	0.1546	1.0403	6.3816
	R^2	0.9459	0.9151	0.9617
	σ	0.2571	0.3220	0.2163
Intraparticle diffusion	k_i, mg g^{-1} min^{-2}	3.3443	0.4573	0.0821
	c_i, mg g^{-1}	29.8260	21.6460	11.8550
	R^2	0.9154	0.7497	0.9561
	σ	0.6119	1.0525	0.4408
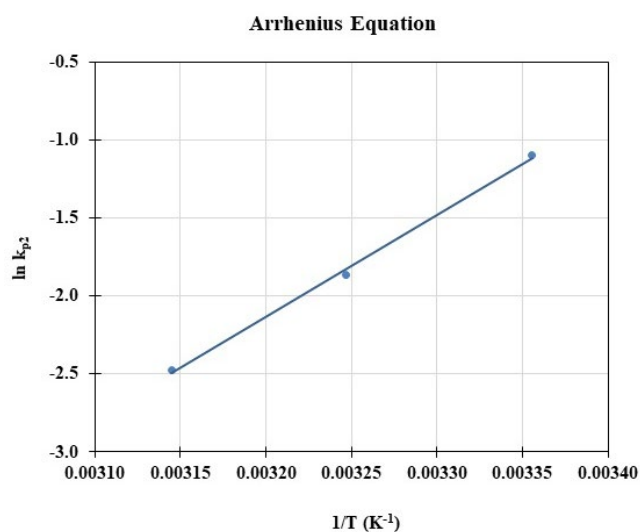
Fig. 9. Arrhenius plot for RB19 adsorption on SC-FA-G2 magnetic nanoadsorbent.

model. The magnitude of E_a can be used for the prediction of the adsorption mechanism. If the activation energy is less than 40 kJ/mole, the possible mechanism of the adsorption process could be physical in nature. Oppositely, higher activation energies are needed for the chemical adsorption process (40–800 kJ/mole) [44,82,83]. In the present study, the activation energy value (E_a) was determined by using k_{p2} values obtained from the pseudo-second-order kinetic that was found the best fitted model to the adsorption data (Fig. 9). E_a value was calculated as 54.443 kJ/mole with the correlation coefficient of $R^2 = 0.9989$ and the standard deviation of $\sigma = 0.0447$. As the value of E_a calculated is higher than 40 kJ/mole, the rate-limiting step in the RB19 dye adsorption onto the SC-FA-G2 process may be associated with the chemically controlled mechanism.

3.7. Recovery efficiency of magnetic nanoadsorbent

The adsorption performance and the regeneration of adsorbents are the important parameters in practical applications. Especially, adequate repeated uses are the most significant parameter for studying from the economic point of view [22,35]. In the present study, 0.1 mole/L NaOH solution was used to recover RB19 dye onto novel magnetic nanoadsorbent, SC-FA-G2. As the pH of the solution increases, the number of negatively charged sites increases, which aids the desorption of RB19 dye [84].

The recovery efficiency values of the regenerated SC-FA-G2 obtained for each adsorption–desorption cycle are represented in Fig. 10. As can be seen from this figure, RB19 dye removal efficiencies were calculated as 100% and 96% in the first and tenth adsorption–desorption cycles, respectively. This result refers that the regenerated nanoadsorbent still has a high recovery efficiency even after the tenth adsorption–desorption cycle. Then, it was concluded that the novel magnetic nanoadsorbent, SC-FA-G2, could be easily regenerated after its separation from the solution by using a magnet, and that can be reused again and again as an efficient nanoadsorbent.

In the literature, several researchers studied RB19 dye adsorption from aqueous solutions onto various adsorbent types such as some agricultural and industrial wastes, organic or inorganic based materials, and etc. The findings obtained from these studies and the present study are summarized in Table 6.

4. Conclusions

In the present study, IMANC synthesized by solution combustion method using stoichiometric amount of glycine as fuel, with a porous surface area of 19.69 m²/g and particle size of 60 nm, as reported in our previous study [70], was examined as novel magnetic nanoadsorbent for removal of RB19 dye which is one of the dyestuffs mostly used in the
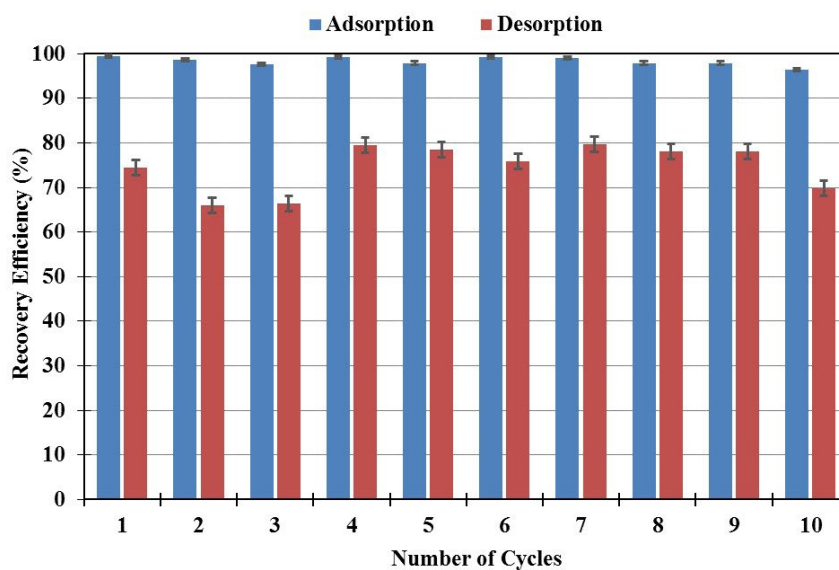

Fig. 10. Recovery efficiency of regenerated SC-FA-G2 for each adsorption-desorption cycle.

Table 6
Comparison of the removal percentages of RB19 dye onto various adsorbents at optimum process conditions

Reference	Adsorbent	Optimum conditions						Maximum adsorption capacity (q_m, mg/g)	Adsorption isotherm model	Adsorption kinetic model
		Adsorbent amount (g/L)	Initial dye conc. (mg/L)	Time (min)	Temp. (°C)	pH	Dye removal (%)			
Ahmed et al. [18]	CTAB-modified OP	4	20–300	60	30	4	–	100	Temkin	Pseudo-second-order
	CTAB-modified SOP			60			–	166.6	Temkin	
Nga et al. [36]	Nanostructured magnesium oxide particles	0.1	50	20	18	7	99	250	Langmuir	–
Radaei et al. [1]	Activated carbon	1.025	100	6.8	–	11	98.1	–	–	–
Nguyen and Pho [2]	Chitosan coated magnetic hydroxyapatite nanoparticles	2	50	–	–	6	93	–	–	–
Rafiee and Jahangiri-rad [37]	Multi-walled carbon nanotube	0.6	20 - 200	120	50	3	–	450	Liu	–
	Single-walled carbon nanotube							550		
Khoshhesab and Ahmadi [39]	NiO nanoparticles	2.2	75	60	25	–	–	–	Sips model	Pseudo-second-order
Malakootian et al. [40]	Alumina/carbon nanotube	0.4	30	180	25	3	93.51	–	Freundlich	Pseudo-second-order
Karimifard et al. [42]	Multi-walled carbon nanotubes	0.65	100	20	–	3	98.11	53.3	–	–
Dalvand et al. [43]	L-arginine-functionalized Fe_3O_4 nanoparticles	0.74	50		–	3	96.34	125	Freundlich	Pseudo-second-order
Ciobanu et al. [44]	Uncalcined HAP nanopowders	2	65	180	20	3	95.58	90.1	Langmuir	Pseudo-second-order
	Calcined HAP nanopowders						86.95	74.9		
Mousa and Taha [13]	Activated carbon	5	100	300	–	6.5	90.50	–	Langmuir	Pseudo-second-order
Abbasi [46]	Chitosan/SiO$_2$/carbon nanotubes	1	50	–	–	2	98	97.1	Langmuir	Pseudo-second-order
Banaei et. al. [47]	Modified silica gel	0.4	20	30	45	4	98.32	72.9	Langmuir	Pseudo-second-order
Xu et al. [22]	Chitosan-based magnetic adsorbent	5	100	–	30	2	90.00	–	Langmuir	–
Azizi et al. [48]	Graphene oxide modified with polystyrene	1	20	120	23	7	–	39.1	Freundlich	Elovich
Present Study	Iron based magnetic aluminium oxide nanocomposite, IMANC (SC-FA-G2)	8	100	4	25	2	96.5	55.2	Langmuir	Pseudo-second-order
		8		30	45		97.7			
		12		2	35		100			

textile industry. The main findings obtained from the present study on the RB19 dye adsorption onto SC-FA-G2 were summarized as follows:

- The experimental set of RB19 dye removal was planned using a Design Expert 11.0 trial software experimental design programme according to RSM. The maximum RB19 dye removal (100%) was observed under the process conditions as follows; (i) pH of 2, 25°C, and 400 mg SC-FA-G2/50 mL; (ii) pH of 2, 35°C, and 600 mg SC-FA-G2/50 mL; and (iii) pH of 2, 45°C, and 400 mg SC-FA-G2/50 mL for 60 min of processing time.
- The quadratic model was developed using the Box–Behnken design method to explain the relationship between the process parameters chosen and the process response. The most effective parameters on RB19 dye removal were found as pH and nanoadsorbent amount. But, the effect of temperature was found less significant on RB19 dye removal compared to other parameters investigated.
- After evaluation of the data obtained from dye adsorption studies, the Langmuir adsorption isotherm model was found as the most appropriate model with a higher value of correlation coefficient ($R^2 = 0.9956$) and lower value of standard deviation ($\sigma = 0.0275$). The maximum adsorption capacity value (q_m) was calculated as 55.25 mg/g. The separation factor, R_L (0.024), for Langmuir isotherm showed that SC-FA-G2 was favorable for the RB19 dye adsorption.
- After evaluation of the data obtained from the kinetic studies, the pseudo-second-order kinetic model was found as the most appropriate model with a higher value of correlation coefficient ($R^2 = 0.9999$) and a lower value of standard deviation ($\sigma = 0.0045$).
- Arrhenius equation was used for calculation of the activation energy for the dye adsorption by using pseudo-second-order rate constants and found as 54.443 kJ/mole. The activation energy (E_a) obtained higher than 40 kJ/mole indicated that the adsorption process is chemical sorption.
- The parameters obtained from the isotherm, kinetic and Arrhenius models suggested that the chemisorption is the possible mechanism of the dye molecules adsorption process onto SC-FA-G2.
- The maximum dye recovery values were obtained at dramatically shorter processing times at the optimum process conditions. For example, the maximum dye removal percentages at the temperature values of 25°C, 35°C, and 45°C were found as 96.5%, 100%, and 97.7% for 4, 2, and 30 min of processing time at the nanoadsorbent amounts of 8, 12, and 8 g/L, respectively.
- The recovery efficiency of the regenerated SC-FA-G2 was found as 96% even after the tenth adsorption–desorption cycle.

Finally, the findings refer that SC-FA-G2 has remarkable features such as high adsorption capacity, easy regeneration and adequate repeated uses for removal of RB19 dye. Data showed that SC-FA-G2 could be utilized efficiently as a novel magnetic nanoadsorbent for the removal of anionic dyes from aqueous solutions. The extremely effective and reusable features of the novel magnetic nanoadsorbent give valuable information to the researchers who work on the environmental sciences and to the industrial companies for eliminating this dye from wastewaters. For further studies, the potential usage of SC-FA-G2 as a promising alternative nanoadsorbent could be evaluated for the removal of various materials such as other textile or non-textile dyes, pesticides, heavy metals or other environmental pollutants from wastewater.

Acknowledgment

References

[1] E. Radaei, M.R.A. Moghaddam, M. Arami, Removal of Reactive Blue 19 from aqueous solution by pomegranate residual-based activated carbon: optimization by response surface methodology, J. Environ. Health Sci. Eng., 12 (2014) 1–8.

[2] V.C. Nguyen, Q.H. Pho, Preparation of chitosan coated magnetic hydroxyapatite nanoparticles and application for adsorption of Reactive Blue 19 and Ni²⁺ ions, Sci. World J., 2014 (2014) 1–9.

[3] M.R. Mafra, L. Igarashi-Mafra, D.R. Zuim, É.C. Vasques, M.A. Ferreira, Adsorption of remazol brilliant blue on an orange peel adsorbent, Braz. J. Chem. Eng., 30 (2013) 657–665.

[4] Y. Shiferaw, J.M. Yassin, A. Tedla, Removal of organic dye and toxic hexavalent chromium ions by natural clay adsorption, Desal. Water Treat., 165 (2019) 222–231.

[5] M. Dehvari, M. Ghaneian, A. Ebrahimi, B. Jamshidi, M. Mootab, Removal of Reactive Blue 19 dyes from textile wastewater by pomegranate seed powder: isotherm and kinetic studies, Int. J. Environ. Health Eng., 5 (2016) 1–9.

[6] S. Rashid, C. Shen, J. Yang, J. Liu, J. Li, Preparation and properties of chitosan–metal complex: some factors influencing the adsorption capacity for dyes in aqueous solution, J. Environ. Sci., 66 (2018) 301–309.

[7] K.C. Lai, L.Y. Lee, B.Y.Z. Hiew, S. Thangalazhy-Gopakumar, S. Gan, Environmental application of three-dimensional graphene materials as adsorbents for dyes and heavy metals: review on ice-templating method and adsorption mechanisms, J. Environ. Sci., 79 (2018) 174–199.

[8] S. Natarajan, H.C. Bajaj, R.J. Tayade, Recent advances based on the synergetic effect of adsorption for removal of dyes from waste water using photocatalytic process, J. Environ. Sci., 65 (2018) 201–222.

[9] M. Wiśniewska, M. Wawrzkiewicz, E. Polska-Adach, G. Fijałkowska, O. Goncharuk, Nanosized silica–titanium oxide as a potential adsorbent for C.I. Acid Yellow 219 dye removal from textile baths and wastewaters, Appl. Nanosci., 8 (2018) 867–876.

[10] T.Y. Kim, S.Y. Cho, Adsorption equilibria of reactive dye onto highly polyaminated porous chitosan beads, Korean J. Chem. Eng., 22 (2005) 691–696.

[11] K. Ghosh, N. Bar, A.B. Biswas, S.K. Das, Removal of Methylene Blue (aq) using untreated and acid-treated *Eucalyptus* leaves and GA-ANN modeling, Can. J. Chem. Eng., 97 (2019) 2883–2898.

[12] S. Farias, D. De Oliveira, A.A. Ulson De Souza, S.M.A.G.U. De Souza, A.F. Morgado, Removal of Reactive Blue 21 and Reactive Red 195 dyes using horseradish peroxidase as catalyst, Braz. J. Chem. Eng., 34 (2017) 701–707.

[13] K.M. Mousa, A.H. Taha, Adsorption of Reactive Blue dye onto natural and modified wheat straw, J. Chem. Eng. Process Technol., 6 (2015) 9.

[14] M.R. Patil, S.D. Khairnar, V.S. Shrivastava, Synthesis, characterisation of polyaniline–Fe₃O₄ magnetic nanocomposite and its application for removal of an acid violet 19 dye, Appl. Nanosci., 6 (2016) 495–502.

[15] M.R. Patil, V.S. Shrivastava, Adsorption of malachite green by polyaniline–nickel ferrite magnetic nanocomposite: an isotherm and kinetic study, Appl. Nanosci., 5 (2015) 809–816.

[16] K. Sharma, R.K. Vyas, A.K. Dalai, Thermodynamic and kinetic studies of Methylene Blue degradation using reactive adsorption and its comparison with adsorption, J. Chem. Eng. Data, 62 (2017) 3651–3662.

[17] M.M. Mustafa, P. Jamal, M.F. Alkhatib, S.S. Mahmod, D.N. Jimat, N.N. Ilyas, Panus tigrinus as a potential biomass source for Reactive Blue decolorization: isotherm and kinetic study, Electron. J. Biotechnol., 26 (2017) 7–11.

[18] S.A. Ahmed, L.B. Khalil, T. El-Nabarawy, Removal of Reactive Blue 19 dyes from aqueous solution using natural and modified orange peel, Carbon Lett., 13 (2012) 212–220.

[19] M.B. Mohamadi, H. Ejazi, F. Azadbakht, Using composite chitosan-graphene oxide to eliminate Reactive Blue 19 from water solutions: the study of adsorption kinetics and reaction thermodynamics, Desal. Water Treat., 155 (2019) 341–349.

[20] Y.H. Lee, S.G. Pavlostathis, Decolorization and toxicity of reactive anthraquinone textile dyes under methanogenic conditions, Water Res., 38 (2004) 1838–1852.

[21] D. Balarak, Y. Mahdavi, A. Joghatayi, The application of low-cost adsorbent for Reactive Blue 19 dye removal from aqueous solution: *Lemna minor*, Arch. Hyg. Sci., 4 (2015) 199–207.

[22] B. Xu, H. Zheng, H. Zhou, Y. Wang, K. Luo, C. Zhao, Y. Peng, X. Zheng, Adsorptive removal of anionic dyes by chitosan-based magnetic microspheres with pH-responsive properties, J. Mol. Liq., 256 (2018) 424–432.

[23] S. Sadri Moghaddam, M.R. Alavi Moghaddam, M. Arami, Coagulation/flocculation process for dye removal using sludge from water treatment plant: optimization through response surface methodology, J. Hazard. Mater., 175 (2010) 651–657.

[24] J.C. Edwards, Investigation of Color Removal by Chemical Oxidation for Three Reactive Textile Dyes and Spent Textile Dye Wastewater, Virginia Polytechnic Institute and State University, Environmental Science and Engineering Department, Master in Science Thesis, Blacksburg, Virginia, 2000.

[25] C. Suksaroj, M. Héran, C. Allègre, F. Persin, Treatment of textile plant effluent by nanofiltration and/or reverse osmosis for water reuse, Desalination, 178 (2005) 333–341.

[26] M. Weng, Z. Zhou, Q. Zhang, Electrochemical degradation of typical dyeing wastewater in aqueous solution: performance and mechanism, Int. J. Electrochem. Sci., 8 (2013) 290–296.

[27] R.S. Gowri, R. Vijayaraghavan, P. Meenambigai, Microbial degradation of reactive dyes-a review, Int. J. Curr. Microbiol. Appl. Sci., 3 (2014) 421–436.

[28] S. Wijannarong, S. Aroonsrimorakot, P. Thavipoke, C. Kumsopa, S. Sangjan, Removal of reactive dyes from textile dyeing industrial effluent by ozonation process, APCBEE Procedia, 5 (2013) 279–282.

[29] S. Karcher, A. Kornmüller, M. Jekel, Anion exchange resins for removal of reactive dyes from textile wastewaters, Water Res., 36 (2002) 4717–4724.

[30] E. Worch, Adsorption Technology in Water Treatment-Fundamentals, Processes and Modeling, DE GRUYTER, Germany, 2012.

[31] M.A.M. Salleh, D.K. Mahmoud, W.A.W.A. Karim, A. Idris, Cationic and anionic dye adsorption by agricultural solid wastes: a comprehensive review, Desalination, 280 (2011) 1–13.

[32] J. Xu, Z. Cao, Y. Zhang, Z. Yuan, Z. Lou, X. Xu, X. Wang, A review of functionalized carbon nanotubes and graphene for heavy metal adsorption from water: preparation, application, and mechanism, Chemosphere, 195 (2018) 351–364.

[33] Y. Peng, D. Xiao, G. Yu, Y. Feng, J. Li, X. Zhao, Y. Tang, L. Wang, Q. Zhang, Effect of an eco-friendly o/w emulsion stabilized with amphiphilic sodium alginate derivatives on lambda-cyhalothrin adsorption–desorption on natural soil minerals, J. Environ. Sci., 78 (2019) 230–238.

[34] M. Mondal, K. Manoli, A.K. Ray, Removal of arsenic(III) from aqueous solution by concrete-based adsorbents, Can. J. Chem. Eng., 98 (2019) 353–359.

[35] M. Asgher, H.N. Bhatti, Removal of Reactive Blue 19 and reactive blue 49 textile dyes by *citrus* waste biomass from aqueous solution: equilibrium and kinetic study, Can. J. Chem. Eng., 90 (2012) 412–419.

[36] N.K. Nga, P.T.T. Hong, T.D. Lam, T.Q. Huy, A facile synthesis of nanostructured magnesium oxide particles for enhanced adsorption performance in Reactive Blue 19 removal, J. Colloid Interface Sci., 398 (2013) 210–216.

[37] M. Rafiee, M. Jahangiri-rad, Adsorption of Reactive Blue 19 from aqueous solution by carbon nanotubes:equilibrium, thermodynamics and kinetic studies, Res. J. Environ. Sci., 8 (2014) 205–2014.

[38] M.T. Ghaneian, M.H. Ehrampoush, F. Sahlabadi, M. Mootab, I. Rezapour, T. Jasemizad, Reactive Blue 19 dye adsorption behavior on jujube stems powder from synthetic textile wastewater: isotherm and kinetic adsorption studies, J. Community Health Res., 3 (2014) 67–78.

[39] M.Z. Khoshhesab, M. Ahmadi, Removal of Reactive Blue 19 from aqueous solutions using NiO nanoparticles: equilibrium and kinetic studies, Desal. Water Treat., 57 (2015) 20037–20048.

[40] M. Malakootian, H.J. Mansoorian, A. Hosseini, N. Khanjani, Evaluating the efficacy of alumina/carbon nanotube hybrid adsorbents in removing Azo Reactive Red 198 and Blue 19 dyes from aqueous solutions, Process Saf. Environ. Prot., 96 (2015) 125–137.

[41] A.A. El-Bindary, M.A. Abd El-Kawi, A.M. Hafez, I.G.A. Rashed, E.E. Aboelnaga, Removal of Reactive Blue 19 from aqueous solution using rice straw fly ash, J. Mater. Environ. Sci., 7 (2016) 1023–1036.

[42] S. Karimifard, M.R. Alavi Moghaddam, Enhancing the adsorption performance of carbon nanotubes with a multistep functionalization method: optimization of Reactive Blue 19 removal through response surface methodology, Process Saf. Environ. Prot., 99 (2016) 20–29.

[43] A. Dalvand, R. Nabizadeh, M. Reza Ganjali, M. Khoobi, S. Nazmara, A. Hossein Mahvi, Modeling of Reactive Blue 19 azo dye removal from colored textile wastewater using L-arginine-functionalized Fe_3O_4 nanoparticles: optimization, reusability, kinetic and equilibrium studies, J. Magn. Magn. Mater., 404 (2016) 179–189.

[44] G. Ciobanu, S. Barna, M. Harja, Kinetic and equilibrium studies on adsorption of Reactive Blue 19 dye from aqueous solutions by nanohydroxyapatite adsorbent, Arch. Environ. Prot., 42 (2016) 3–11.

[45] E. Demirhan, Removal of Reactive Blue 19 from aqueous solution by peanut shell:optimization by response surface methodology, Selcuk Univ. J. Eng., Sci. Technol., 5 (2017) 312–321.

[46] M. Abbasi, Synthesis and characterization of magnetic nanocomposite of chitosan/SiO_2/carbon nanotubes and its application for dyes removal, J. Cleaner Prod., 145 (2017) 105–113.

[47] A. Banaei, S. Samadi, S. Karimi, H. Vojoudi, E. Pourbasheer, A. Badiei, Synthesis of silica gel modified with 2,2′-(hexane-1,6-diylbis(oxy)) dibenzaldehyde as a new adsorbent for the removal of Reactive Yellow 84 and Reactive Blue 19 dyes from aqueous solutions: equilibrium and thermodynamic studies, Powder Technol., 319 (2017) 60–70.

[48] A. Azizi, E. Moniri, A.H. Hassani, H. Ahmad Panahi, M. Miralinaghi, Polymerization of graphene oxide with polystyrene: non-linear isotherms and kinetics studies of anionic dyes, Microchem. J., 145 (2019) 559–565.

[49] Y.L. Huang, D.S. Xue, P.H. Zhou, Y. Ma, F.S. Li, α-Fe-Al_2O_3 nanocomposites prepared by sol–gel method, Mater. Sci. Eng., A, 359 (2003) 332–337.

[50] W. Liu, W. Zhong, H. Jiang, N. Tang, X. Wu, Y. Du, Highly stable alumina-coated iron nanocomposites synthesized by wet chemistry method, Surf. Coat. Technol., 200 (2006) 5170–5174.

[51] M.F. Alajmi, J. Ahmed, A. Hussain, T. Ahamad, N. Alhokbany, S. Amir, T. Ahmad, S.M. Alshehri, Green synthesis of Fe_3O_4 nanoparticles using aqueous extracts of *Pandanus odoratissimus* leaves for efficient bifunctional electro-catalytic activity, Appl. Nanosci., 8 (2018) 1427–1435.

[52] D. Demir, D. Güreş, T. Tecim, R. Genç, N. Bölgen, Magnetic nanoparticle-loaded electrospun poly(ε-caprolactone) nano-fibers for drug delivery applications, Appl. Nanosci., 8 (2018) 1461–1469.

[53] X. Ren, H. Chen, V. Yang, D. Sun, Iron oxide nanoparticle-based theranostics for cancer imaging and therapy, Front. Chem. Sci. Eng., 8 (2014) 253–264.

[54] D. Lin, L. Kong, K. Chen, J. He, T. Liu, Y. Li, X. Cai, Y. Hu, K. Zhang, J. Liu, Removal of cadmium and lead ions from water by sulfonated magnetic nanoparticle adsorbents, J. Colloid Interface Sci., 494 (2017) 307–316.

[55] K. Pandi, N. Viswanathan, In-situ fabrication of magnetic iron oxide over nano-hydroxyapatite gelatin eco-polymeric composite for defluoridation studies, J. Chem. Eng. Data, 61 (2016) 571–578.

[56] M.A. Karakassides, D. Gournis, A.B. Bourlinos, P.N. Trikalitis, T. Bakas, Magnetic Fe_2O_3-Al_2O_3 composites prepared by a modified wet impregnation method, J. Mater. Chem., 13 (2003) 871–876.

[57] M. Munoz, Z.M. de Pedro, N. Menendez, J.A. Casas, J.J. Rodriguez, A ferromagnetic γ-alumina-supported iron catalyst for CWPO. Application to chlorophenols, Appl. Catal., B, 136–137 (2013) 218–224.

[58] O.V. Makarchuk, T.A. Dontsova, I.M. Astrelin, Magnetic nanocomposites as efficient sorption materials for removing dyes from aqueous solutions, Nanoscale Res. Lett., 11 (2016) 1–7.

[59] T. Huang, M. Yan, K. He, Z. Huang, G. Zeng, A. Chen, M. Peng, H. Li, L. Yuan, G. Chen, Efficient removal of methylene blue from aqueous solutions using magnetic graphene oxide modified zeolite, J. Colloid Interface Sci., 543 (2019) 43–51.

[60] G.Z. Kyzas, K.A. Matis, Nanoadsorbents for pollutants removal: a review, J. Mol. Liq., 203 (2015) 159–168.

[61] A. Murray, B. Örmeci, Competitive effects of humic acid and wastewater on adsorption of Methylene Blue dye by activated carbon and non-imprinted polymers, J. Environ. Sci., 66 (2018) 310–317.

[62] A. Bevilacqua, M.R. Corbo, M. Sinigaglia, Design of Experiments: A Powerful Tool in Food Microbiology, A. Mendez-Vilas, Ed., Curr. Res. Technol. Educ. Top. Appl. Microbiol. Microb. Biotechnol., Ser. No.2 Vol.1, Formatex Research Center, Badajoz, Spain, 2010.

[63] M. Mäkelä, Experimental design and response surface methodology in energy applications: a tutorial review, Energy Convers. Manage., 151 (2017) 630–640.

[64] K. Ravikumar, K. Pakshirajan, T. Swaminathan, K. Balu, Optimization of batch process parameters using response surface methodology for dye removal by a novel adsorbent, Chem. Eng. J., 105 (2005) 131–138.

[65] R. Rajeshkannan, N. Rajamohan, M. Rajasimman, Removal of malachite green from aqueous solution by sorption on *hydrilla verticillata* biomass using response surface methodology, Front. Chem. Eng. China, 3 (2009) 146–154.

[66] N. Aslan, Y. Cebeci, Application of Box-Behnken design and response surface methodology for modeling of some Turkish coals, Fuel, 86 (2007) 90–97.

[67] A. Hadi, J. Karimi-Sabet, A. Dastbaz, Parametric study on the mixed solvent synthesis of ZIF-8 nano- and micro-particles for CO adsorption: a response surface study, Front. Chem. Sci. Eng., (2019) 1–16.

[68] B.K. Nandi, A. Goswami, M.K. Purkait, Adsorption characteristics of brilliant green dye on kaolin, J. Hazard. Mater., 161 (2009) 387–395.

[69] M. Mourabet, A. El Rhilassi, H. El Boujaady, M. Bennani-Ziatni, A. Taitai, Use of response surface methodology for optimization of fluoride adsorption in an aqueous solution by Brushite, Arabian J. Chem., 10 (2017) S3292–S3302.

[70] M. Pehlivan, S. Simsek, S. Ozbek, B. Ozbek, An extensive study on the synthesis of iron based magnetic aluminium oxide nanocomposites by solution combustion method, J. Mater. Res. Technol., 8 (2019) 1746–1760.

[71] M. Siddique, R. Farooq, A. Shaeen, Removal of Reactive Blue 19 from wastewaters by physicochemical and biological processes-a review, J. Chem. Soc. Pak., 33 (2011) 284–293.

[72] F. Çiçek, D. Özer, A. Özer, A. Özer, Low cost removal of reactive dyes using wheat bran, J. Hazard. Mater., 146 (2007) 408–416.

[73] H. Masitah, H.H. Bassim, A. Abdul Latif, Thermodynamic Studies on Removal of Reactive Blue 19 Dye on Cross-linked Chitosan/Oil Palm Ash Composite Beads, 3rd International Conference on Energy and Environment (ICEE), IEEE, Malacca, Malaysia, 2009, pp. 50–54.

[74] C.A. Igwegbe, L. Mohmmadi, S. Ahmadi, A. Rahdar, D. Khadkhodaiy, R. Dehghani, S. Rahdar, Modeling of adsorption of Methylene Blue dye on Ho-$CaWO_4$ nanoparticles using response surface methodology (RSM) and artificial neural network (ANN) techniques, MethodsX, 6 (2019) 1779–1797.

[75] F. Ghorbani, S. Kamari, Application of response surface methodology for optimization of methyl orange adsorption by Fe-grafting sugar beet bagasse, Adsorpt. Sci. Technol., 35 (2017) 317–338.

[76] B.K. Aziz, D.M. Salh, S. Kaufhold, P. Bertier, The high efficiency of anionic dye removal using Ce-Al_{13}/pillared clay from Darbandikhan natural clay, Molecules, 24 (2019) 2720.

[77] W. Konicki, M. Aleksandrzak, D. Moszyński, E. Mijowska, Adsorption of anionic azo-dyes from aqueous solutions onto graphene oxide: equilibrium, kinetic and thermodynamic studies, J. Colloid Interface Sci., 496 (2017) 188–200.

[78] M.J. Iqbal, M.N. Ashiq, Adsorption of dyes from aqueous solutions on activated charcoal, J. Hazard. Mater., 139 (2007) 57–66.

[79] G. Vijayalakshmi, B. Ramkumar, S.C. Mohan, Isotherm and kinetic studies of Methylene Blue adsorption using activated carbon prepared from teak wood waste biomass, J. Appl. Sci., 19 (2019) 827–836.

[80] P. Senthil Kumar, C. Vincent, K. Kirthika, K. Sathish Kumar, Kinetics and equilibrium studies of Pb^{2+} in removal from aqueous solutions by use of nano-silversol-coated activated carbon, Braz. J. Chem. Eng., 27 (2010) 339–346.

[81] Y. Gao, Q. Yue, B. Gao, Comparison on physical, chemical, and adsorption properties of activated carbon derived from different solid wastes, Desal. Water Treat., 57 (2016) 15503–15514.

[82] M.A. Mahmoud, Kinetics and thermodynamics of aluminum oxide nanopowder as adsorbent for Fe(III) from aqueous solution, Beni-Suef Univ. J. Basic Appl. Sci., 4 (2015) 142–149.

[83] E.I. Unuabonah, K.O. Adebowale, B.I. Olu-Owolabi, Kinetic and thermodynamic studies of the adsorption of lead(II) ions onto phosphate-modified kaolinite clay, J. Hazard. Mater., 144 (2007) 386–395.

[84] F. Güzel, H. Sayğili, G.A. Sayğili, F. Koyuncu, Elimination of anionic dye by using nanoporous carbon prepared from an industrial biowaste, J. Mol. Liq., 194 (2014) 130–140.